Microtubule growth activates Rac1 to promote lamellipodial protrusion in fibroblasts

Clare M. Waterman-Storer*‡, Rebecca A. Worthylake†, Betty P. Liu†, Keith Burridge† and E.D. Salmon*

*Department of Biology, University of North Carolina, Chapel Hill, North Carolina 27599, USA
†Department of Cell Biology/Anatomy and Lineberger Comprehensive Cancer Center, University of North Carolina, Chapel Hill, North Carolina 27599, USA
‡e-mail: waterman@email.unc.edu

Microtubules are involved in actin-based protrusion at the leading-edge lamellipodia of migrating fibroblasts. Here we show that the growth of microtubules induced in fibroblasts by removal of the microtubule destabilizer nocodazole activates Rac1 GTPase, leading to the polymerization of actin in lamellipodial protrusions. Lamellipodial protrusions are also activated by the rapid growth of a disorganized array of very short microtubules induced by the microtubule-stabilizing drug taxol. Thus, neither microtubule shortening nor long-range microtubule-based intracellular transport is required for activating protrusion. We suggest that the growth phase of microtubule dynamic instability at leading-edge lamellipodia locally activates Rac1 to drive actin polymerization and lamellipodial protrusion required for cell migration.

Migrating fibroblasts in culture exhibit an elongated, polarized shape, with a wide flat lamella that terminates in a ruffling lamellipodium at the leading edge, facing the direction of migration, and a trailing cell body tapering back to an extended tail[1]. The tapering cell sides are relatively inactive. Membrane protrusions and ruffles are continuously initiated at the leading edge and undergo a smooth centripetal movement, known as retrograde flow, towards the cell body[1]. Localized actin polymerization, nucleated at the leading edge, is required for ruffling activity, retrograde flow and protrusion of the leading edge to drive directed cell migration[2]. Microtubules emanate out from the cell centre towards the leading edge, aligned with the direction of migration, where their plus ends exhibit random changes between periods of growth and shortening; such fluctuations are termed dynamic instability[3]. When treated with agents that cause microtubule disassembly, fibroblasts lose their extended shape, and the protrusive lamellipodial activity that is normally confined to the leading edge is reduced and distributed to random sites around the cell periphery[4,5]. Thus, microtubules are thought to promote lamellipodial protrusion and direct sites of actin polymerization[6]. Indeed, correlative video and immunofluorescence microscopy has shown that when microtubules enter a protrusion of the leading edge, the edge becomes stabilized against retraction, so promoting the cell's forward advance[7].

The prevailing hypothesis is that microtubules, extending from the cell centre to the leading edge, serve as tracks for the directed delivery of membrane vesicles to the lamellipodium, where the membrane of the vesicles is inserted into the plasma membrane at the leading edge to drive lamellipodial protrusion and retrograde flow during cell migration[8–10]. However, cell migration is stopped by pharmacological stabilization of microtubule dynamic instability without disassembly of microtubule tracks, indicating that migration requires some aspect of microtubule dynamic instability[11]. We show here that the induction of microtubule polymerization by removal of the microtubule-destabilizing drug nocodazole causes activation of the small GTPase Rac1 in fibroblasts, leading to actin polymerization in lamellipodial protrusions. Rac1 is also activated when microtubule growth is promoted and microtubule shortening is blocked by the microtubule stabilizer taxol. Thus, the growth phase of microtubule dynamic instability can activate a signal-transduction cascade that induces lamellipodial protrusion to drive cell migration.

Results

To investigate how microtubules contribute to lamellipodial protrusion and membrane ruffling in fibroblasts, we used multimode digital imaging microscopy to simultaneously observe the dynamics of fluorescent microtubules and cell-shape changes in kinetic studies of recovery from treatment with nocodazole. We plated Swiss 3T3 or NIH3T3 fibroblasts into growth medium containing 10 μM nocodazole, incubated the cells overnight, microinjected them with X-rhodamine-labelled tubulin and mounted them in a perfusion chamber for high-resolution time-lapse digital imaging.

Microtubule growth after nocodazole washout induces lamellipodial protrusion. Before perfusion of nocodazole-free medium to induce microtubule growth, cells were irregular in shape and not elongated, with small areas of protrusive ruffling at random sites totalling 9.3% of their peripheries, as observed by phase-contrast microscopy (Fig. 1, time 00:00; Fig. 2a; see Supplementary Information). Cells in nocodazole exhibited very little retrograde flow, and organelles underwent brownian movement in the cytoplasm. As shown by epifluorescence microscopy, X-rhodamine tubulin was diffusely localized throughout the cell (Fig. 1, time 00:00). Within seconds after perfusion of nocodazole-free media, microtubules began to grow primarily by nucleation at the centrosome next to the nucleus, but also from non-centrosomal sites (Fig. 1, time 2:15; see Supplementary Information). Microtubules grew out from the cell centre with their plus ends leading, and upon reaching the periphery (usually within ~10 min), their lengths began oscillating between 5 and 10 μm between the growth and shortening phases of dynamic instability. Microtubules in the cell periphery sometimes bent and grew parallel to the cell edge, making visible their retrograde movement towards the cell centre[12]. Following microtubule growth, phase-contrast images showed that the nucleus rotated or repositioned so that it was directly apposed to the centrosome. Organelles began directed saltatory motions, and mitochondria moved out towards the cell periphery (Fig. 1; see Supplementary Information). These nuclear and organellar movements were most likely driven by microtubule-based motor activity[13].

Surprisingly, within 113 ± 87 s (n=10) of nocodazole washout, ruffling lamellipodial protrusions were initiated at various sites, making up ~50% of the cell periphery. This was a rapid response to microtubule growth that was not expected from results of previous studies[4,5] (Fig. 1 and Fig. 2a; see Supplementary Information). Most lamellipodial protrusions advanced, widened and fused with adjacent protrusions, while a few protrusions subsided. Advancing protrusions induced a 15–20% increase in cell perimeter at both 2 and 20 min after perfusion (Fig. 2b). Microtubule plus ends grew into the advancing protrusions (Fig. 1, times 4:30–37:49). This activity continued as the cell gained an extended polarized shape, within 45–60 min. Similar reactions were observed after ultraviolet-light-induced inactivation of colchicine, another microtubule-depolym-

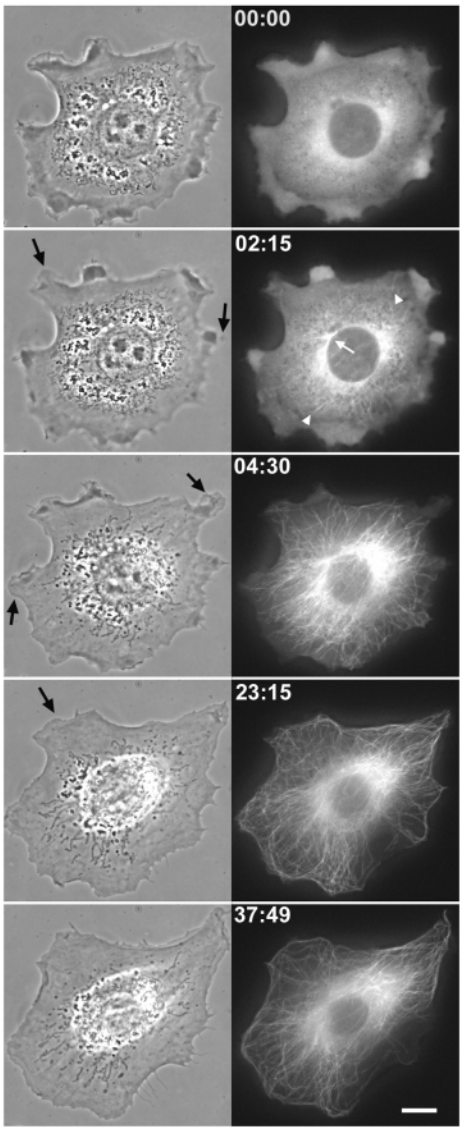

Figure 1 **Microtubule and cellular dynamics in cells after washout of 10 μM nocodazole in an NIH3T3 fibroblast.** See also Supplementary Information. The time elapsed since nocodazole washout is shown in min:s; scale bar represents 10 μm. X-rhodamine-labelled tubulin is shown in the right panels; the corresponding phase-contrast images, acquired within 1 s of the fluorescence images, are shown in the left panels. At time 00:00, after ~16 h in 10 μM nocodazole, the cell is not elongated, and labelled tubulin is diffuse in the cytoplasm. At 2:15 after nocodazole washout, microtubules nucleate from both centrosomal (white arrow) and non-centrosomal (white arrowheads) sites, and protrusions of the cell edge have begun (black arrows). Protrusions, filled with microtubule ends, continue to advance, widen, and extend the area of the cell (times 4:30–37:58).

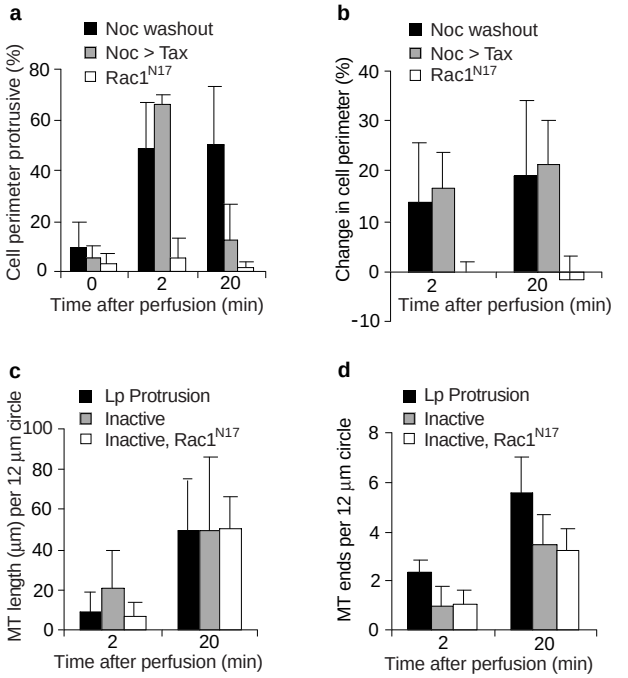

Figure 2 **Quantification of lamellipodial protrusion, cell spreading and microtubule organization during recovery from nocodazole treatment in fibroblasts. a**, Lamellipodial protrusion, expressed as the percentage of the cell perimeter undergoing protrusive activity (see Methods), just before perfusion with nocodazole-containing medium (time 0) and at 2 and 20 min after nocodazole washout (black bars), exchange from 10 μM nocodazole into 10 μM taxol medium (grey bars) or nocodazole washout in cells injected with Rac1^{N17} (white bars). Nocodazole washout induced a sustained increase in protrusive activity. Exchange from nocodazole into taxol medium induced a transient increase in lamellipodial protrusion that subsided by 20 min. Rac1^{N17} inhibited lamellipodial protrusion induced by nocodazole washout. 0 min: nocodazole washout 9.3 ± 10.0%, n=10; exchange from nocodazole into taxol 5.7 ± 1.5%, n=6; nocodazole washout, Rac1^{N17}, 3.0 ± 3.9%, n=12. 2 min: nocodazole washout 48.9 ± 17.8%, n=10; exchange from nocodazole into taxol 65.5 ± 6.8%, n=6; nocodazole washout, Rac1^{N17}, 5.5 ± 7.8%, n=12. 20 min: nocodazole washout 50.1 ± 22.5%, n=10; exchange from nocodazole into taxol 12.8 ± 3.8%, n=6; nocodazole washout, Rac1^{N17}, 1.2 ± 2.7%, n=12. **b**, Change in cell perimeter, expressed as a percentage of the perimeter length before perfusion (see Methods) compared at 2 and 20 min after nocodazole washout (black bars), exchange from 10 μM nocodazole into 10 μM taxol medium (grey bars) or nocodazole washout in cells injected with Rac1^{N17} (white bars). For nocodazole washout and exchange from nocodazole into taxol media, the cell perimeter increased over time. This cell spreading was inhibited after nocodazole washout in cells injected with Rac1^{N17}. 2 min: nocodazole washout 13.9 ± 11.8%, n=10; exchange from nocodazole into taxol 16.6 ± 2.0%, n=6; nocodazole washout, Rac1^{N17}, 0.08 ± 1.6%, n=12. 20 min: nocodazole washout 18.8 ± 15.4%, n=10; exchange from nocodazole into taxol 21.2 ± 6.6%, n=6; nocodazole washout, Rac1^{N17}, –1.6 ± 4.8%, n=12. **c**, **d**, Total microtubule length (**c**) or number of microtubule ends (**d**) within a 6-μm radius at lamellipodial protrusions (black bars) and at inactive cell edges (grey bars) (see Methods) at 2 and 20 min after nocodazole washout. **c**, Total microtubule-polymer length is similar at lamellipodial protrusions and inactive cell edges. There is no difference in the total microtubule length after nocodazole washout at inactive cell edges in control cells and in cells injected with Rac1^{N17}. **d**, The number of microtubule ends is greater at lamellipodial protrusions than at inactive edges. There is no difference in the number of microtubule ends after nocodazole washout between inactive cell edges in control cells and cells injected with Rac1^{N17}. **c**, 2 min: protruding edge 4.6 ± 4.5 μm and inactive edge 10.2 ± 9.7 μm, n=16 cells; inactive edge, Rac1^{N17}, 7.1 ± 7.1 μm, n=12 cells. 20 min: protruding edge 24.7 ± 12.6 μm and inactive edge 24.9 ± 17.9 μm, n=16 cells; inactive edge, Rac1^{N17}, 50.2 ± 15.9 μm, n=12 cells. **d**, 2 min: protruding edge 2.3 ± 1.0 ends; inactive edge 1.0 ± 1.6 ends, n=16 cells; inactive edge, Rac1^{N17}, 1.1 ± 0.6 ends, n=12 cells. 20 min: protruding edge 5.6 ± 2.9 ends and inactive edge 3.5 ± 2.3 ends, n=16 cells; inactive edge, Rac1^{N17}, 3.2 ± 0.9, n=12 cells. MT, microtubule.

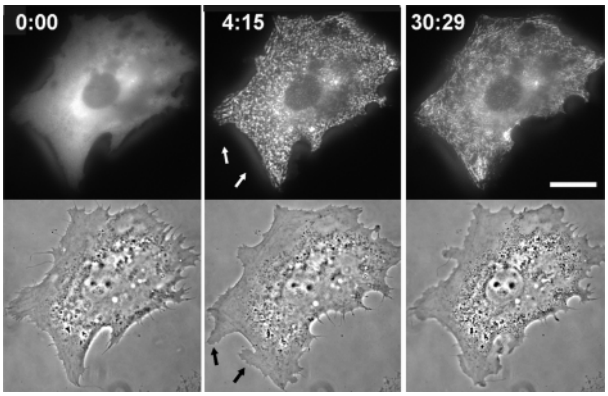

Figure 3 **Microtubule and cellular dynamics in an NIH3T3 cell during exchange from medium containing 10 μM nocodazole into medium containing 10 μM taxol.** See also Supplementary Information. The time after perfusion of medium containing 10 μM taxol is shown in min:s; scale bar represents 15 μm. X-rhodamine-labelled tubulin is shown in top panels; the corresponding phase-contrast images, acquired within 1 s of the fluorescence images, are shown in bottom panels. Before medium exchange (time 0:00), the cell is irregular in shape and labelled tubulin is diffuse in the cytoplasm. By 4:15 after exchange of media, protruding ruffles have extended (arrows), but the short microtubules that formed immediately after perfusion have not entered the protrusions. By 30:29, protrusion ceases and the ruffles retract.

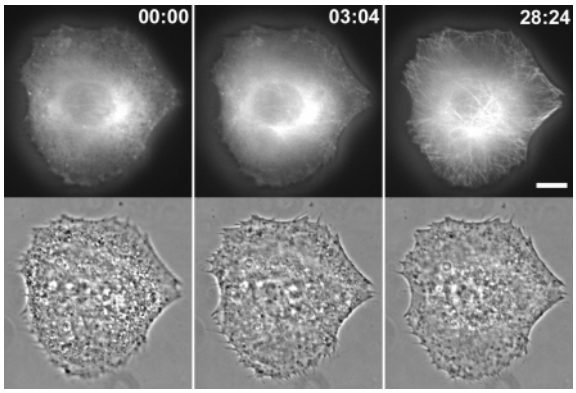

Figure 5 **Nocodazole washout in a Swiss 3T3 cell injected with Rac1^{N17}.** See Supplementary Information. Time after nocodazole washout is shown in min:s; scale bar represents 15 μm. X-rhodamine-labelled microtubules are shown in top panels; the corresponding phase-contrast images, acquired within 1 s of the fluorescence images, are shown in bottom panels. The nocodazole-treated cell shown was microinjected with Rac1^{N17} 32 min before imaging. Following nocodazole washout, microtubules nucleate at centrosomal and non-centrosomal sites (time 03:04) and grow to the cell periphery (time 28:24). However, ruffling and protrusion of the cell periphery are completely inhibited after nocodazole washout (times 03:04 and 28:24).

erizing drug (data not shown). Perfusion of nocodazole-containing media did not promote protrusive ruffling activity (data not shown).

We next investigated whether the length of the microtubule polymer or the number of microtubule plus ends correlated with lamellipodial protrusion. To approach this question, we determined the total microtubule length and the number of microtubule plus ends within a 6-μm radius of either sites of lamellipodial protrusion or inactive edges at 2 and 20 min after nocodazole washout. There was no significant difference in the total microtubule-polymer length at protruding or inactive edges (Fig. 2c). However, there were significantly (P<0.05) more microtubule plus ends at protruding edges compared with at inactive edges, both at 2 min (2.3 ± 1.1 ends at protruding edges, 1.0 ± 1.6 at inactive edges, n=17) and, particularly, at 20 min (5.5 ± 2.9 ends at protruding edges, 3.5 ± 2.3 at inactive edges, n=17) after nocodazole washout (Fig. 2d). Thus, the sites of lamellipodial protrusion correlate with areas of the cell at which dynamic microtubule plus ends are concentrated.

Taxol-induced microtubule growth activates protrusion. To determine whether either directed microtubule-based intracellular transport or microtubule dynamic instability was required for microtubule-polymerization-induced lamellipodial protrusion, we analysed cells during perfusion from medium containing 10 μM nocodazole into medium containing 10 μM taxol. Taxol induces non-centrosomal microtubule nucleation and inhibits dynamic instability by blocking microtubule disassembly and markedly promoting microtubule growth[14]. Immediately after exchange from nocodazole- into taxol-containing medium, there was an extremely rapid and massive nucleation of very short microtubules throughout the cytoplasm (Fig. 3; see Supplementary Information). Microtubules grew to only ~2–3 μm in length, had no organization, did not exhibit retrograde flow, and underwent brownian movement in the cytoplasm. In addition, the nucleus did not reposition, and organelles continued to exhibit brownian motion in the cytoplasm and never showed any directed motility. In spite of this, lamellipodial protrusions formed along 65.5 ± 6.8% of the cell perimeter within 2 min after exchange from nocodazole- into taxol- containing media (Fig. 2a), and the cell spread (Fig. 2b). However, the small microtubules did not detectably increase in length after their initial polymerization and never entered the protrusions (Fig. 3, arrows). Furthermore, membrane protrusions were transient and subsided by 20 min after perfusion to 12.8 ± 3.8% of the cell periphery, a value similar to that obtained in nocodazole-containing medium before perfusion (Fig. 2a). The cells never established polarity. Thus, lamellipodial protrusion can be transiently activated by the growth of very short, disorganized microtubules in the absence of directed intracellular organelle transport.

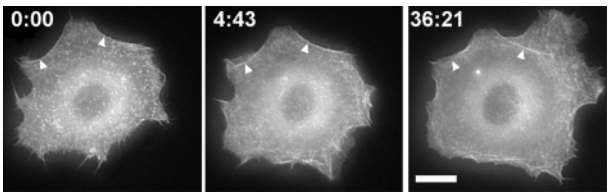

Figure 4 **F-actin dynamics during nocodazole washout in a Swiss 3T3 cell.** See Supplementary Information. The time after nocodazole washout is shown in min:s; scale bar represents 15 μm. The cell was injected with X-rhodamine-labelled actin. In these images, G-actin appears as diffuse background staining, and F-actin appears as brightly staining filamentous structures. At time 0:00, actin is concentrated in puncta and peripheral arcs (arrowheads). At 4:43 and 36:21, actin assembly occurs in advancing protrusions while older actin structures (arrowheads) remain stationary and intact.

Microtubule growth after nocodazole washout induces actin polymerization. To test whether lamellipodial protrusions induced by microtubule growth are produced by changes in actin assembly or F-actin organization, we imaged fluorescent actin dynamics in cells by microinjection of X-rhodamine-labelled actin, and then washed out nocodazole from the medium. In fibroblasts that were incubated overnight in nocodazole and injected with labelled actin (which was allowed to incorporate into cellular structures for at least 2 h), there were few stress fibres and labelled actin localized in cytoplasmic punctae and concave arcs at the cell periphery (Fig. 4, time 0:00). Following nocodazole washout, actin was incorporated at the leading edge of protrusions, and pre-existing actin structures such as arcs and punctae, as well as new structures within forming

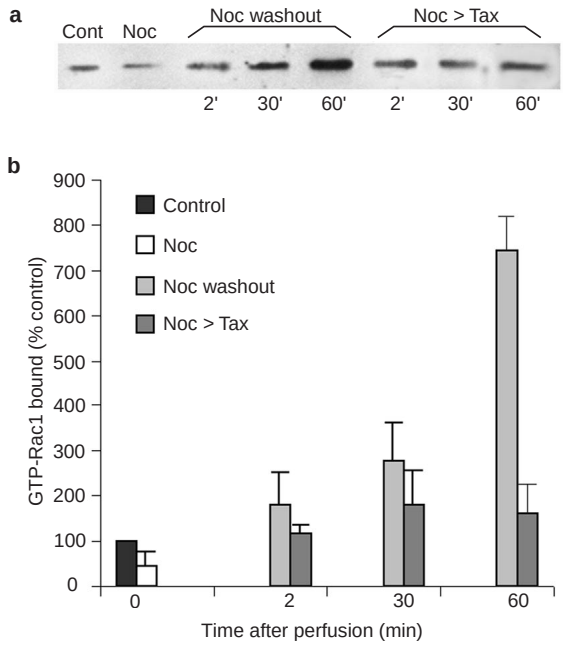

Figure 6 **Microtubule growth activates Rac1.** Comparison of Rac1 activity between control cells (Cont), cells treated overnight with 10 μM nocodazole (Noc), and cells treated overnight with 10 μM nocodazole then sampled at 2, 30 and 60 min after nocodazole washout (Noc washout) or exchange from nocodazole- into taxol-containing media (Noc>Tax). **a**, A representative anti-Rac1-probed immunoblot of precipitated Rac1-GTP from cell lysates. **b**, Quantification of signal in blots, corrected for total Rac1 level in the cell lysates and shown relative to control cells in serum-containing media. Results are the averages obtained from two experiments. Treatment with 10 μM nocodazole overnight results in a reduction in Rac1-GTP to 44.2 ± 31.0% compared with untreated cells. Two min after nocodazole washout or exchange from 10 μM nocodazole- into 10 μM taxol-containing medium, Rac1-GTP levels increased to 180.5 ± 80.2% and 113.5 ± 70.0% of control values, respectively. After nocodazole washout, Rac1-GTP levels continued to rise to 277.0 ± 70.2% and 742.9 ± 84.8% of control values at 30 and 60 min post-washout, respectively. In contrast, after exchange from nocodazole- into taxol-containing medium, Rac1-GTP amounts levelled off and decreased to 180.2 ± 20.9% and 161.9 ± 74.8% of control values at 30 and 60 min after perfusion, respectively.

protrusions, remained intact (Fig. 4, times 4:43 and 36:21; see Supplementary Information). Thus microtubule growth activates the *de novo* assembly of F-actin at the cell periphery to induce the formation of lamellipodial protrusions, as opposed to recruiting pre-existing F-actin from other structures.

Rac1 mediates protrusion induced by microtubule growth. The microtubule-growth-induced lamellipodial protrusions and assembly of F-actin that we have observed in fibroblasts are remarkably similar to the ruffling lamellipodia that are induced to form by activation of the small GTPase Rac1 (ref. 15,16). Rac1 is a member of the Rho family of small GTPases that cycle between active GTP-bound forms and inactive GDP-bund forms[17]. Rac1 is activated by stimulation of membrane receptors with serum agonists such as platelet-derived growth factor (PDGF) or insulin[18].

To determine whether signalling through Rac1 is involved in the activation of lamellipodial protrusion by microtubule growth, we analysed the effects of nocodazole washout on cells injected with a mutant form of Rac1, $Rac1^{N17}$, that acts as a dominant inhibitor of Rac1 activity[19]. In contrast to control cells, cells injected with $Rac1^{N17}$ showed no induction of lamellipodial protrusion (Fig. 2a), cell spreading (Fig. 2b) or retrograde flow (Fig. 5; see Supplementary Information) after nocodazole washout. Microtubule nucleation and growth after nocodazole washout in cells injected with $Rac1^{N17}$ proceeded similarly to in control cells after nocodazole washout, and neither the total microtubule polymer length nor the number of microtubule ends near inactive cell edges differed significantly between $Rac1^{N17}$ and control cells (Fig. 2c, d). However, microtubules did not exhibit retrograde flow upon reaching the cell periphery after nocodazole washout in $Rac1^{N17}$-injected cells. The nucleus repositioned and organelles began directed saltatory movement, indicating that microtubule-based motility was not affected by $Rac1^{N17}$; however, cell polarity was never established. These results indicate that dominant-negative Rac1 inhibits lamellipodial protrusion induced by microtubule growth.

Microtubule growth activates Rac1. To determine whether microtubule polymerization results in activation of Rac1 or relieves some inhibition downstream of active Rac1, we studied directly the amount of GTP-bound Rac1 in fibroblasts after induction of microtubule growth (Fig. 6a, b). To measure Rac1 activity, we used an affinity assay to precipitate Rac1-GTP from cell lysates[20]. In this assay, a fragment of p65/p21-activated kinase ($p65^{PAK}$), a Rac1 effector that binds with high affinity to Rac1-GTP but not to Rac1-GDP[21], was used to construct an affinity matrix. Using this assay, we found that overnight treatment of fibroblasts with nocodazole decreased the amount of Rac1-GTP to 44 ± 31% (n=2) of values for control cells in serum-containing media. Two minutes after the initiation of microtubule polymerization by nocodazole washout, we detected an increase of 180 ± 70% (n=2) in the amount of Rac1-GTP compared with controls. Rac1-GTP levels continued to increase, to 277 ± 69% (n=2) and 743 ± 84% (n=2) of control values at 30 and 60 min after nocodazole washout, respectively. Similarly, 2 min after exchange from nocodazole- into taxol-containing media, the amount of Rac1 increased to 113 ± 65% (n=2) of control levels. However, after transfer from nocodazole- into taxol-containing medium the level of Rac1-GTP did not continue to rise. Instead, it rose to 180 ± 20% (n=2) and decreased to 162 ± 70% (n=2) of control values at 30 and 60 min post-perfusion, respectively. Thus, depolymerization of microtubules by overnight incubation in nocodazole reduces Rac1-GTP levels in fibroblasts, despite the presence of extracellular Rac1-activating factors in the serum. The subsequent induction of microtubule growth induces an increase in Rac1-GTP amounts.

Discussion

Our results provide, to our knowledge, the first insights into the molecular mechanism of microtubule-mediated promotion of lamellipodial protrusion during fibroblast migration. The prevailing hypothesis proposes that directed microtubule-based vesicle transport from the cell centre to the leading edge and subsequent localized vesicle exocytosis are required for lamellipodial protrusion and retrograde flow[8–10]. In contrast, our results show that the growth of microtubules activates Rac1, which in turn drives actin polymerization and ruffling lamellipodial protrusion at the leading edge. Furthermore, we have shown that protrusion and ruffling are transiently activated by the rapid growth of a disorganized array of very short microtubules by taxol. These taxol-induced microtubules are much too short to extend from the cell centre to the periphery and do not support long-range, directed intracellular transport of organelles to the cell edge, as observed by phase-contrast microscopy. Thus, protrusion of the leading edge can occur independently of microtubule-based organelle transport. However, the long-term maintenance of protrusive activity and the establishment of fibroblast polarity may also require that microtubules are organized into a radial array.

Our results also shed light on why microtubule dynamic instability is important for cell migration. When microtubule polymerization was induced by nocodazole washout, a steady-state equilibrium between tubulin dimers and polymers was reached within ~10 min, as indicated by the onset of plus-end dynamic instability, with microtubules switching between growth and short-

ening phases near the cell edges. However, a massive burst of microtubule growth induced by taxol perfusion also produced lamellipodial protrusion, indicating that the activation of protrusion is independent of microtubule shortening and the concentration of free tubulin dimers, but requires microtubule growth. Because taxol-induced protrusion was transient, the maintenance of protrusions seems to require fresh microtubule growth. Thus, microtubule dynamic instability is a mechanism to create a constant supply of freshly growing microtubule plus ends to the cell periphery. This steady pool of growing microtubule ends could in turn continuously induce local activation of Rac1 to promote lamellipodial protrusion, actin polymerization and retrograde flow at the cell edge to drive cell migration. This mechanism also explains why the location of lamellipodial protrusion is correlated with high concentrations of dynamically unstable microtubule plus ends at the cell edge rather than high concentrations of microtubule polymer *per se*. However, it is unclear why Rac1 activity continued to rise when the amount of microtubule polymer in cells appeared to have reached steady-state levels. Levels of Rac1 activity remained raised after microtubule polymerization by taxol, during the time when taxol-induced protrusions were retracting, so the return to baseline levels after a pulse in Rac1 activity is not immediate, and takes over an hour.

How does the growth phase of microtubule dynamic instability activate Rac1? One possibility is that microtubule growth directly generates cytoplasmic Rac1-GTP. Rac1-GTP, but not Rac1-GDP, can bind to tubulin dimers[22]. Thus, if Rac1-GTP and tubulin were to compete for the same binding site on a microtubule, it is possible that Rac1-GTP could be displaced from tubulin and released into the cytoplasm when the tubulin is added to the end of a microtubule during growth. This would explain how growing microtubule ends could provide active Rac1 to the leading cell edge. Alternatively, there is biochemical evidence to indicate that microtubules may enhance Rac1 activity by mediating the assembly of microtubule-bound Rac1 signalling complexes. Indeed, both upstream guanine-nucleotide-exchange-factor activators of Rac1, including GEF-H1 (ref. 23), Vav[24] and Lfc[25], and the downstream Rac1 effectors MLK2 and JNK[26] either bind to tubulin or localize to microtubules in cells[19]. It is also possible that these signalling complexes could associate preferentially with growing microtubule plus ends *in vivo*, making their assembly dependent on microtubule growth, similar to the behaviour observed for the microtubule–endosome linking protein, CLIP-170 (ref. 27). Finally, it may be that the activity of some other Rho-family member is responsible for microtubule-growth-dependent Rac1 activity. RhoG activates both Rac1 and the Rho-family member Cdc42Hs in a microtubule-dependent way[28]. Thus, microtubule-growth-induced lamellipodial protrusions could be due to RhoG activity. However, it is not clear how RhoG activity could depend on fresh microtubule growth.

Another member of the Rho family of GTPases, RhoA, is also important in the relationship between microtubules and F-actin in cell contractility and adhesion. RhoA inhibitors block the assembly of F-actin stress fibres and the formation of focal adhesions that are induced by microtubule depolymerization[29–31]. Not surprisingly, direct measurement of RhoA-GTP levels in cells has also shown that depolymerization of microtubules with colchicine activates RhoA[32]. This observation, together with our results, indicates that Rho-family members may underlie the elusive crosstalk between microtubules and actin that is required for the regulation of cell motility and cytokinesis[33]. □

Methods

Cell culture and microinjection.

NIH3T3 or Swiss 3T3 mouse fibroblasts were plated onto coverslips in growth media containing 10 μM nocodazole and 10% fetal bovine serum ('nocodazole media') at 37 °C in 5% CO_2 and incubated overnight. Cells were microinjected with 2 mg ml^{-1} X-rhodamine-labelled tubulin (in 50 mM potassium glutamate, 0.5 mM $MgCl_2$, pH 7.0), 1 mg ml^{-1} X-rhodamine-labelled actin (in 2 mM Tris, 0.2 mM $CaCl_2$, 0.2 mM ATP, 0.5 mM BME, pH 7), or a combination of 1 mg ml^{-1} X-rhodamine labelled tubulin and 5 mg ml^{-1} $Rac1^{N17}$ (in 50 mM potassium glutamate, 5 mM $MgCl_2$, 25 mM KCl, 1 μM GDP, pH 7)[12,34,35]. X-rhodamine-labelled tubulin and actin were prepared from porcine brain and chicken breast muscle as described and labelled with a succinimidyl ester of X-rhodamine (Molecular Probes)[34]. $Rac1^{N17}$ was expressed as a fusion protein with glutathione-*S*-transferase (GST) in *Escherichia coli* and purified by glutathione affinity[35]. $Rac1^{N17}$ was cleaved from the glutathione affinity matrix with thrombin, and excess thrombin was removed by para-aminobenzamidine affinity. Purified $Rac1^{N17}$ appeared as a single band of relative molecular mass 21,000 on an overloaded SDS–PAGE gel stained with Coomassie brilliant blue (data not shown). Cells were allowed to recover from microinjection before imaging for 30–180 min while still in nocodazole media at 37 °C.

Multimode digital microscopy.

Coverslips of injected cells were mounted in a custom-built perfusion chamber in nocodazole media containing Oxyrase to inhibit photobleaching[12] (Oxyrase Inc., Ashland, OH) and imaged with a Nikon ×60 1.4 NA phase-contrast objective with a cooled charge-coupled-device camera (Hamamatsu C4880) on a digital multimode microscope system[36]. Illumination was shuttered between exposures. Electronic shutters and image acquisition were under the control of Metamorph software (Universal Imaging, Westchester, PA). Sample temperature was maintained at 35–37 °C with an air-stream stage incubator (Nevtek, Burnsville, VA). Pairs of phase-contrast and epifluorescence images were collected within 1.5 s of each other at 7-s intervals for 5–10 min before perfusion and up to 90 min after perfusion.

Image analysis.

Micrographs were calibrated from images of a stage micrometer, and all length measurements were made using analysis functions in Metamorph software[12]. There were no significant differences in the results obtained with NIH3T3 versus Swiss 3T3 cells, so results for both cell types were pooled. To determine the degree of cell spreading, the cell perimeter was traced and its length determined just before and at 2 and 20 min after perfusion. The state of activity of the cell edge was determined by viewing time-lapse sequences. A series of 11 images (corresponding to ~80 s) were viewed as a movie loop; the sixth image in the series corresponded to the time point being analysed. An area of the cell edge was considered inactive if it did not protrude or retract during the 11 frames, whereas it was considered protruding if it extended and remained extended during the 11-frame loop. The total of length measurements of microtubules or the total number of microtubule ends was determined within a circle of 6-μm radius placed on the image so as to be bisected by the cell edge, at either a protruding or an inactive area of the cell edge.

Rac1-activity assay.

The Rac-activity assay was done essentially as described[20]. NIH3T3 cells were lysed at 37 °C (so that microtubules remained intact) in 50 mM Tris, 150 mM NaCl, 1% Triton-X100, 0.5% deoxycholate, pH 7.5. GTP-bound Rac1 was affinity-precipitated from cell lysates at 4 °C by using an immobilized GST fusion of the Rac1-binding domain of murine $p65^{PAK}$ (the 'PAK binding domain' (PBD), corresponding to amino acids 29–90) that binds Rac1-GTP but not Rac1-GDP[21]. Bound proteins were separated by 15% SDS–PAGE and immunoblotted with anti-Rac1 antibodies (Transduction Labs). The blots were imaged with a digital camera (Eagle Eye, Stratagene), and the signal in images of the blots was quantified using Metamorph software, corrected for total Rac1 levels in the cell lysates, and shown graphically relative to the corrected signal in control cells.

RECEIVED 8 FEBRUARY 1999; REVISED 22 MARCH 1999; ACCEPTED 26 MARCH 1999; PUBLISHED MAY 1999.

1. Heath, J. P. & Holifield, B. F. Cell locomotion: new research tests old ideas on membrane and cytoskeletal flow. *Cell Motil. Cytoskeleton* **18,** 245–257 (1991).
2. Mitchison, T. J. & Cramer, L. P. Actin-based cell motility and cell locomotion. *Cell* **84,** 371–379 (1996).
3. Desai, A. & Mitchison, T. J. Microtubule polymerization dynamics. *Annu. Rev. Cell Dev. Biol.* **13,** 83–117 (1997).
4. Vasiliev, J. M. *et al.* Effect of colcemid on the locomotory behaviour of fibroblasts. *J. Embryol. Exp. Morph.* **24,** 625–690 (1970).
5. Bershadsky, A. D., Vaisberg, E. A. & Vasiliev, J. M. Pseudopodial activity at the active edge of migrating fibroblast is decreased after drug-induced microtubule depolymerization. *Cell Motil. Cytoskeleton* **19,** 152–158 (1991).
6. Vasiliev, J. M. Polarization of pseudopodial activities: cytoskeletal mechanisms. *J. Cell Sci.* **98,** 1–4 (1991).
7. Rinnerthaler, G., Geiger, B. & Small, J. Contact formation during fibroblast locomotion: involvement of membrane ruffles and microtubules. *J. Cell Biol.* **106,** 747–760 (1988).
8. Rodionov, V. I. *et al.* Microtubule-dependent control of cell shape and pseudopodial activity is inhibited by the antibody to kinesin motor domain. *J. Cell Biol.* **123,** 1811–1820 (1993).
9. Bretscher, M. S. Getting membrane flow and the cytoskeleton to cooperate. *Cell* **87,** 601–606 (1996).
10. Singer, S. J. & Kupfer, A. The directed migration of eukaryotic cells. *Annu. Rev. Cell Biol.* **2,** 337–365 (1986).
11. Liao, G., Nagasaki, T. & Gundersen, G. G. Low concentrations of nocodazole interfere with fibroblast locomotion without significantly affecting microtubule level: implications for the role of dynamic microtubules in cell locomotion *J. Cell Sci.* **108,** 3473–3483 (1995).
12. Waterman-Storer, C. M. & Salmon, E. D. Actomyosin-based retrograde flow of microtubules in the lamella of migrating epithelial cells influences microtubule dynamic instability and turnover and is associated with microtubule breakage and treadmilling. *J. Cell Biol.* **139,** 417–434 (1997).
13. Bloom, G. S. & Goldstein, L. S. Cruising along microtubule highways: how membranes move through the secretory pathway. *J. Cell Biol.* **140,** 1277–1280 (1998).
14. Schiff, P. B. & Horwitz, S. B. Taxol stabilizes microtubules in mouse fibroblast cells. *Proc. Natl Acad. Sci. USA* **77,** 1561–1565 (1980).
15. Ridley, A. J. Paterson, H. F., Johnston, C. L., Diekmann, D. & Hall, A. The small GTP-binding protein rac regulates growth factor-induced membrane ruffling. *Cell* **70,** 401–410 (1992).
16. Machesky, L. M. & Hall, A. Role of actin polymerization and adhesion to extracellular matrix in Rac- and Rho-induced cytoskeletal reorganization. *J. Cell Biol.* **138,** 913–926 (1997).
17. Van Aelst, L. & D'Souza-Schorey, C. Rho GTPases and signaling networks. *Genes Dev.* **11,** 2295–

2322 (1997).
18. Nobes, C. D., Hawkins, P., Stephens, L. & Hall, A. Activation of the small GTP-binding proteins rho and rac by growth factor receptors. *J. Cell Sci.* **108,** 225–233 (1995).
19. Nobes, C. D. & Hall, A. Rho, rac, and cdc42 GTPases regulate the assembly of multimolecular focal complexes associated with actin stress fibers, lamellipodia, and filopodia. *Cell* **81,** 53–62 (1995).
20. Bagrodia, S., Taylor, S. J., Jordon, K. A., Van Aelst, L. & Cerione, R. A. A novel regulator of p21-activated kinases. *J. Biol. Chem* **273,** 23633–23636 (1998).
21. Burbelo, P. D., Drechsel, D. & Hall, A. A conserved binding motif defines numerous candidate target proteins for both Cdc42 and Rac GTPases. *J. Biol. Chem.* **270,** 29071–29074 (1995).
22. Best, A., Ahmed, S., Kozma, R. & L. Lim, L. The Ras-related GTPase Rac1 binds tubulin. *J. Biol. Chem* **271,** 3756–3762 (1996).
23. Ren, Y., Li, R., Zheng, Y. & Busch, H. Cloning and characterization of GEF-H1, a microtubule-associated guanine nucleotide exchange factor for Rac and Rho GTPases. *J. Biol. Chem.* **273,** 34954–34960 (1998).
24. Fernandez, J. A. *et al.* Phosphorylation- and actvitation-independent association of the tyrosine kinase Syk and the tyrosine kinase substrates Cbl and Vav with tubulin in B-cells. *J. Biol. Chem.* **274,** 1401–1406 (1999).
25. Glaven, J. A., Whitehead, I., Bagrodia, S., Kay, R. & Cerione, R. A. The Dbl-related protein, Lfc, localizes to microtubules and mediates the activation of Rac signaling pathways in cells. *J. Biol. Chem* **274,** 2279-2285 (1999).
26. Nagata, K. *et al.* The MAP kinase kinase kinase MLK2 co-localizes with activated JNK along microtubules and associates with kinesin superfamily motor KIF3. *EMBO J.* **17,** 149–158 (1998).
27. Perez, F., Diamantopoulos, G. S., Stalder, R. & Kreis, T. E. Clip-170 highlights growing microtubule ends *in vivo*. *Cell* **96,** 517–552 (1999).
28. Gauthier-Rouviere, C. *et al.* RhoG GTPase controls a pathway that independently activates Rac1 and Cdc42 Hs. *Mol. Biol. Cell* **9,** 1379–1394 (1998).
29. Enomoto, T. Microtubule disruption indcues the formation of actin stress fibers and focal adhesions in cultured cells: possible involvement of the Rho signal cascade. *Cell Struct. Funct.* **21,** 317–326 (1996).
30. Zhang, Q., Magnusson, M. K. & Mosher, D. F. Lysophosphatidic acid and microtubule-destabilizing agents stimulate fibronectin matrix assembly through Rho-dependent actin stress fiber formation and cell contraction. *Mol. Biol. Cell* **8,** 1415–1425 (1997).
31. Liu, B., Chrzanowska-Wodnicka, M. & Burridge, K. Microtubule depolymerization induces stress fibers, focal adhesions, and DNA synthesis via the GTP-binding protein Rho. *Cell Adhesion Commun.* **5,** 249–255 (1998).
32. Ren, X.-D., Kiosses, W. B. & Schwartz, M. A. Regulation of the small GTP-binding protein Rho by cell adhesion and the cytoskeleton. *EMBO J.* **18,** 578–585 (1999).
33. Waterman-Storer, C. M. & Salmon, E. D. Positive feedback interactions between microtubule and actin dynamics during cell motility. *Curr. Opin. Cell Biol.* **11,** 61–67 (1999).
34. Waterman-Storer, C. M., Desai, A., Bulinski, J. C. & Salmon, E. D. Fluorescent speckle microscopy, a method to visualize the dynamics of protein assemblies in living cells. *Curr. Biol.* **8,** 1227–1230 (1998).
35. Self, A. J. & Hall, A. Purification of recombinant Rho/Rac/G25K from *Escherichia coli*. *Methods Enzymol.* **256,** 3–10 (1995).
36. Salmon, E. D. *et al.* A high-resolution multimode digital microscope system. *Methods Cell Biol.* **56,** 185–215 (1998).

ACKNOWLEDGEMENTS

We thank S. Earp, C. Der, S. Bagrodia, R. Cerione, B. Kreft, A. Ridley and D. Cheney for their kind contributions of reagents and advice. C.M.W.-S. is a fellow of the Jane Coffin Childs Fund; R.A.W is supported by an NIH grant to the Lineberger Cancer Center. This work was also supported by NIH grants to E.D.S. and K.B.

Correspondence and requests for materials should be addressed to C.M.W.-S.

Supplementary information is available on *Nature Cell Biology*'s World-Wide Web site (http://cellbio.nature.com).